ELSEVIER

PII: S0010-4485(96)00077-2

Computer-Aided Design, Vol. 29, No. 5, pp. 379–391, 1997

Printed in Great Britain
0010-4485/97/$17.00+0.00

# Robust computation of the rotation minimizing frame for sweep surface modeling*

Wenping Wang† and Barry Joe‡

The rotation minimizing frame is superior to the Frenet frame for modeling sweep surfaces [F. Klok, *Computer Aided Geometric Design* **3**, 217–229 (1986)]. However, the existing techniques for computing the rotation minimizing frame either have low approximation degree or are unrobust numerically. We present a method to compute an approximate rotation minimizing frame in a robust and efficient manner. The following problem is studied. Given an axial curve $A(u)$ in space and a 2D cross-section curve $C(v)$, generate a sweep surface $S(u, v) = A(u) + F(u)C(v)$, where $F(u)$ is a rotation minimizing frame defined on $A(u)$. Our method works by approximating $A(u)$ with a $G^1$ circular-arc spline curve and then sweeping $C(v)$ with a rotation minimizing frame along the approximating circular-arc spline curve; the sweep surface thus generated is an approximation of $S(u, v)$. The advantages of this method are: (1) the approximate rotation minimizing frame is computed robustly, with its error being much smaller than would be obtained by Klok's linear method with the same number of segmentations; (2) the sweep surface generated is a NURBS surface if the cross-section curve is a NURBS curve; (3) the method is easily adapted to generating a smooth and closed sweep surface when $A(u)$ is a closed smooth curve.


**Keywords: surface modeling, biarc, NURBS, sweep surface, moving frame**

## INTRODUCTION

### Problem and definitions

#### Problem

Sweeping is a powerful technique to generate surfaces in computer graphics. There has been abundant research in the modeling and rendering of sweep surfaces, such as in References 3, 5, 6, 8, 12, 22, 30. Given an axial curve $A(u)$ in space and a cross-section curve $C(v)$, *a sweep surface* $S(u, v)$ is generated by $S(u, v) = A(u) + F(u)C(v)$, where $F(u)$ is an orthogonal matrix representing a moving frame along $A(u)$. Geometrically, $S(u, v)$ is generated by sweeping $C(v)$ along $A(u)$ with orientation $F(u)$. To simplify discussion, we assume that $C(v)$ is a 2D curve and is always placed in the plane passing through $A(u)$ and with normal vector $A'(u)$ during sweeping; that is, one axis of the frame $F(u)$ is aligned with the tangent vector $A'(u)$. The key problem in sweep surface generation is to determine the moving frame $F(u)$.

In the rest of this section, we will introduce two moving frames that have been commonly used, the Frenet frame and the rotation minimizing frame, and point out their problems that motivated our research.

#### Frenet frame and its variants

The Frenet frame $F(u) = [N(u)\ B(u)\ T(u)]$ is defined on a smooth space curve $A(u)$ with $A'(u) \times A''(u) \neq 0$. Here $N(u)$, $B(u)$, and $T(u)$ are the normal, binormal, and unit tangent vectors of $A(u)$ respectively, and are given by

$$T(u) = \frac{A'(u)}{\| A'(u) \|}, \quad B(u) = \frac{A'(u) \times A''(u)}{\| A'(u) \times A''(u) \|}$$

$$N(u) = B(u) \times T(u) \tag{1}$$

When the axial curve contains curvature-vanishing points where $A'(u) \times A''(u) = 0$, the Frenet frame given by Equation 1 is undefined at such points; for instance, this occurs at an inflection point of a plane curve $A(u)$. Moreover, the Frenet frame could flip abruptly on an S-shaped space curve, causing the sweep surface to be twisted (see *Figure 1a*). To fix the poor behavior of the Frenet frame across an inflection point of a planar curve, a variant of the Frenet frame has been proposed[8,12]. Suppose $A(u)$ is a curve contained in a plane with the unit normal vector $N_0$. Then this modified Frenet frame $\tilde{F}(u) = [\tilde{F}_x(u)\ \tilde{F}_y(u)\ \tilde{F}_z(u)]$ is defined as

$$\tilde{F}_z(u) = A'(u)/\| A'(u) \|, \quad \tilde{F}_y(u) = N_0$$

$$\tilde{F}_x(u) = \tilde{F}_y(u) \times \tilde{F}_z(u) \tag{2}$$

This remedy eliminates effectively the undesirable flipping of the Frenet frame across an inflection point of a regular plane curve.

To deal with general 3D axial curves, it is suggested in Reference 8 that the points on the curve where the Frenet

* The work of the first author was partially supported by a grant from the Research Grant Council of Hong Kong. The work of the second author was partially supported by a grant from the Natural Sciences and Engineering Research Council of Canada.
† Department of Computer Science, University of Hong Kong, Pokfulam Road, Hong Kong
‡ Department of Computing Science, University of Alberta, Edmonton, Alberta, Canada T6G 2H1
*Paper received: 17 February 1996. Revised: 9 August 1996*

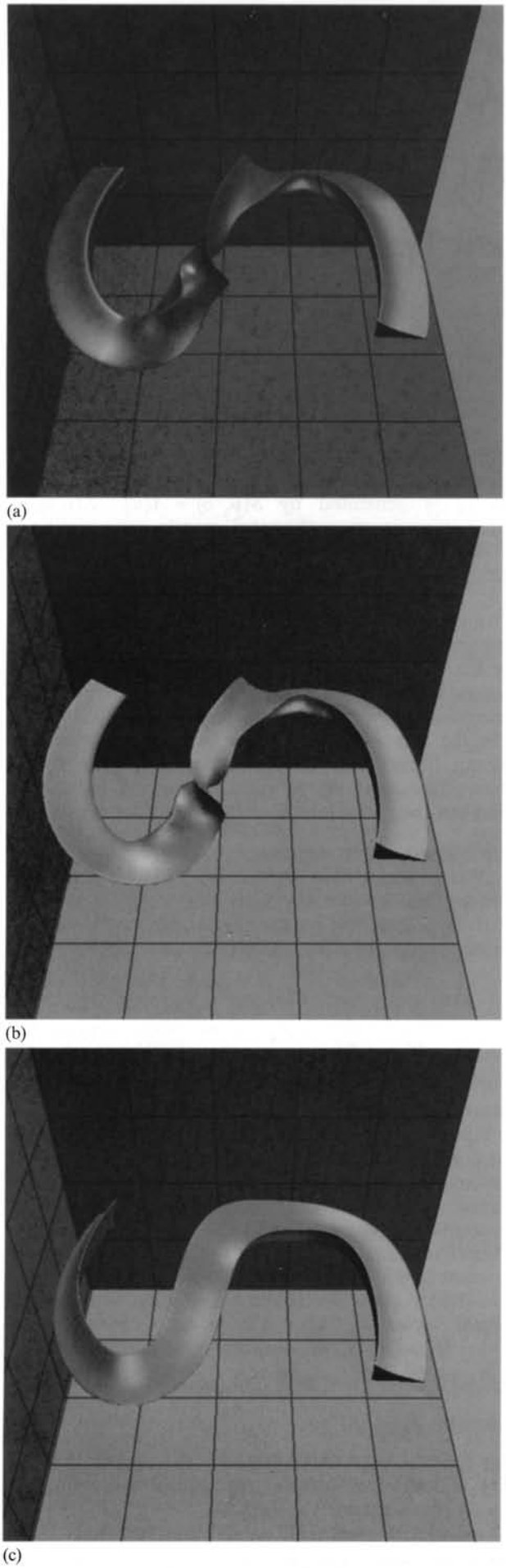

(a)

(b)

(c)

**Figure 1** (a) A surface generated by the Frenet frame. (b) A surface generated by the RMF computed using Equation 4. (c) A surface generated by the biarc method

frame is undefined can be detected and used to divide the curve into segments, and then only Frenet frames over these segments are computed. This method has proved to be effective in some examples shown in Reference 8. But detecting the curvature-vanishing points of a general 3D curve is not a trivial task[15]. Moreover, the frame derived with this method still suffers from other problems, which will be discussed later, of the Frenet frame of a smooth axial curve with non-vanishing curvature.

There is another practical restriction in using the Frenet frame. Note that, for a general space curve, by Equation 1, the continuity of the Frenet frame is the same as that of $A''(u)$. So when $A(u)$ is a cubic B-spline curve, as it is in general only $C^2$ continuous, $F(u)$ will only be $C^0$ continuous, implying that the generated sweep surface $S(u, v)$ will only be $C^0$ continuous. It can be shown that in this case $S(u, v)$ is in general only $G^0$ continuous, i.e. not visually smooth. *Figure 2* shows a $G^0$ sweep surface generated with the Frenet frame along a cubic B-spline curve. (Note that the surface in *Figure 2* looks a little smoother than $G^0$ because of the polygon shading method used.) Therefore, when a visually smooth sweep surface is desired, the use of the Frenet frame will rule out the cubic B-spline curves to be used as axial curves.

**Rotation minimizing frame**

Even for a smooth space curve $A(u)$ with $A'(u) \times A''(u) \neq 0$, the Frenet frame exhibits a certain amount of twist about the tangent of $A(u)$ which is determined by the torsion of the curve and is often unnatural or undesirable. This is best illustrated in *Figure 3a* showing a sweep surface along a free-form curve and in *Plate 1* showing a sweep surface along a torus knot, both generated by the Frenet frame.

To resolve the above problem of the Frenet frame rotating about the axial curve, the *rotation minimizing*

**Figure 2** A $G^0$ surface generated by the Frenet frame along a $C^2$ cubic spline curve

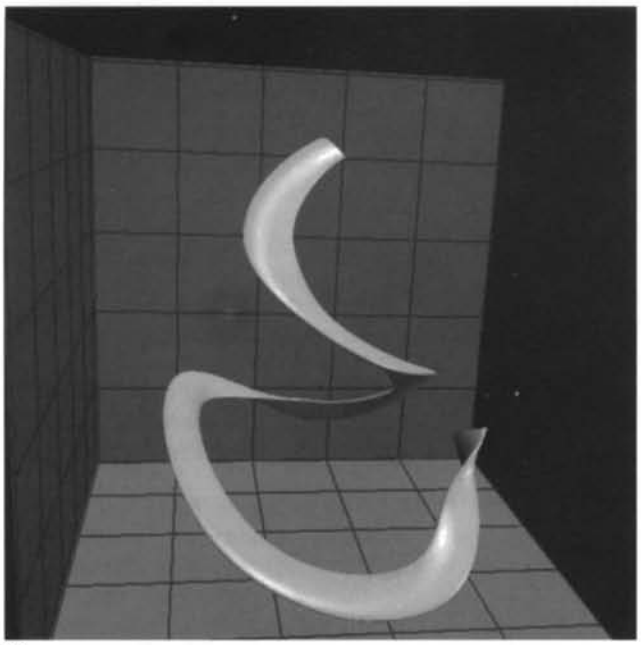

(a)

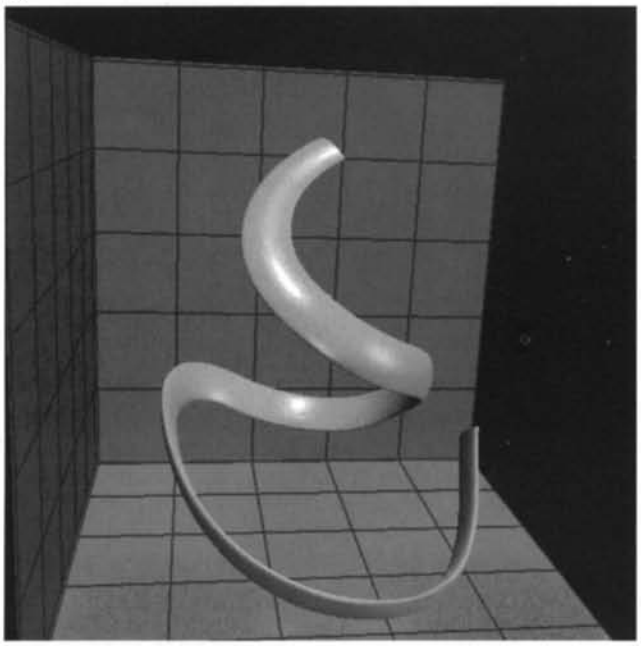

(b)

**Figure 3** (a) A surface generated by the Frenet frame. (b) A surface generated by RMF, computed using the biarc method

*frame* is proposed for sweep surface modeling in Reference 12; an earlier study on the rotation minimizing frame in differential geometry can be found in Reference 2. To contrast with the Frenet frame, a sweep surface which is generated with the rotation minimizing frame is shown in *Figure 3b*, along the same free-form curve *Figure 3a*. In the following the rotation minimizing frame will be referred to as RMF. Let $P(s)$ be an axial curve with arclength parameter $s$. Assume that $P(s)$ is twice differentiable. Denote an RMF of $P(s)$ by $F(s) = [X(s)\ Y(s)\ Z(s)]$, where $Z(s)$ is assigned the unit vector $P'(s)$. Then $X(s)$ and $Y(s)$ are defined to be the solutions of the differential equation

$$V'(s) = -(P''(s) \cdot V(s))P'(s) \tag{3}$$

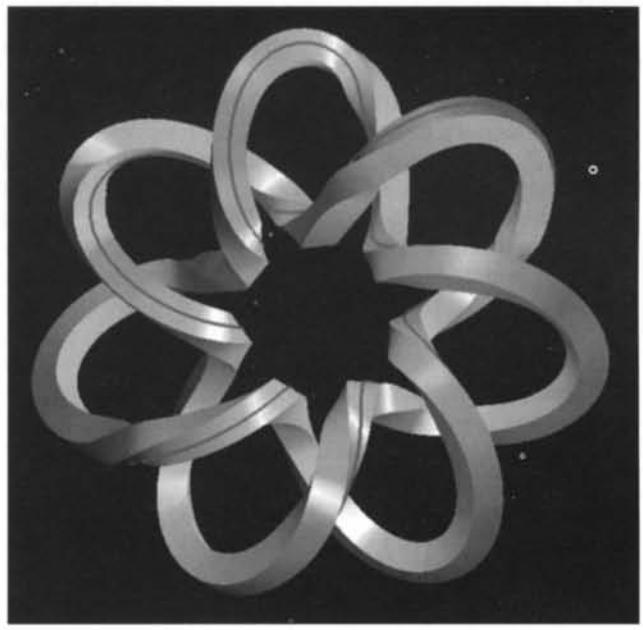

**Plate 1** A surface by the Frenet frame along a torus knot given by $P(t) = ((0.6 + 0.3\cos(7t))\cos(2t),\ (0.6 + 0.3\cos(7t))\sin(2t),\ 0.3\sin(7t))$

with $X(0)$ and $Y(0)$ forming a right-handed orthonormal coordinate frame with $Z(0)$; see Reference 12 for derivation. Different initial vectors $X(0)$ and $Y(0)$ determine different RMFs of $P(s)$, and two RMFs of $P(s)$ differ by a rotation of a constant angle about the tangent of $P(s)$.

An intuitive illustration of the RMF is shown by a sweep surface in *Figure 4* which is generated with a polygonal axial curve and prismatic cross-section curve. Over each straight line segment of the axial curve, the cross-section curve is translated along the segment. This method of computing the RMF along a polygonal curve is proposed in Reference 12.

**Computing rotation minimizing frame**

Although the RMF is readily defined by Equation 3, computing the RMF efficiently and robustly is still a

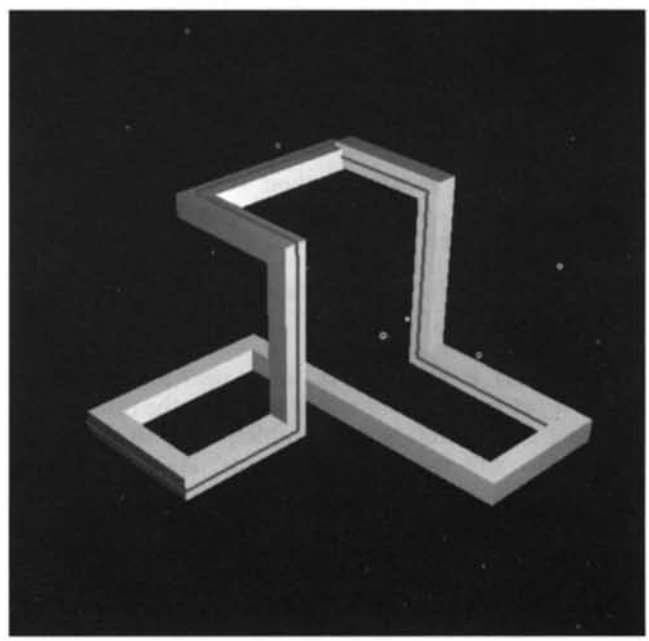

**Figure 4** A rotation minimizing surface along a polygonal curve

problem that has not been solved satisfactorily. Below we review two approaches in literature to computing the RMF.

The first method approximates the axial curve by a polygonal curve and then applies Klok's method[12] to the polygonal axial curve, as described above. This method computes an approximation of the RMF. The *normal plane projection method*, which is essentially the same as Klok's method, is proposed in Reference 25 and is explained in detail in Reference 19. Several other methods of approximating RMF, also based on the polygonal approximation of the axial curve, are suggested in Reference 7. In practice, Klok's method has proven to be numerically robust[7,12]. As we will see later, Klok's method has lower convergence rates than those of our biarc method in both the approximation of the axial curve and the approximation of RMF.

The second method of computing RMF is based on the integral formula for RMF given in Reference 10, which also serves as another definition of RMF. Let an RMF of the axial curve $A(u)$ be $F(u) = [X(u), Y(u), Z(u)]$. Then $Z(u) = A'(u)/ \| A'(u) \|$, and $X(u)$ and $Y(u)$ are given by

$$X(u) = \cos\theta(u)\ N(u) + \sin\theta(u)\ B(u)$$

$$Y(u) = -\sin\theta(u)\ N(u) + \cos\theta(u)\ B(u)$$

with

$$\theta(u) - \theta_0 = -\int_{u_o}^{u} \tau(t) \| A'(t) \| \, dt \tag{4}$$

where $\tau(u)$ is the torsion of $A(u)$. Here $A(u)$ is not necessarily an arclength parameterization. According to the second definition based on integral (4), an RMF is given by rotating the Frenet frame about the tangent of the curve by the angle determined by Equation 4. In other words, the amount of twist of the Frenet frame is equal to the integrated torsion of $A(u)$, and this twist must be compensated by a rotation to convert the Frenet frame to an RMF. (Incidentally, the minus sign in front of the integral in Equation 4 is missing in Reference 10.)

Since for most axial curves the integral (4) cannot be integrated in closed form, numerical integration has to be used to approximate $\theta(u)$. Numerical integration of Equation 4 involves sampling points on $A(u)$ and summing up the values of the integrand at the sampled points, and this in general leads to an approximation of the RMF.

However, this second method suffers from lack of robustness for a general space curve. The torsion in Equation 4 is given by Reference 13:

$$\tau(u) = \frac{\det(A'(u), A''(u), A'''(u))}{\| A'(u) \times A''(u) \|^2}$$

On one hand, evaluating $\tau(u)$ at or near points of $A(u)$ where $A'(u) \times A''(u) = 0$ is unrobust. On the other hand, ignoring such points when sampling $\tau(u)$ in numerical integration will cause a large error. Also, as in this method an RMF is obtained by rotating the Frenet frame, which is used as a reference, the numerically unrobust computation of the Frenet frame, as pointed out in Section 1.1, also makes the second method unrobust. Hence this method cannot be used even for some curves that are smooth and nice by all practical criteria. This is revealed in *Figure 1b* showing a sweep surface generated with this method, using the same axial curve as in *Figure 1a*.

**Biarc method**

We will present an efficient and robust approximate method to model a sweep surface with an RMF along a $G^1$ space curve. The idea is to first approximate the axial curve by a $G^1$ circular-arc spline curve and then generate a sweep surface with an RMF computed along the approximating circular-arc spline curve. The $G^1$ circular-arc spline curve is constructed with biarcs[20,23,28] and so has desirable flexibility for approximation. Finally, as we will see, computing an RMF along a circular-arc spline curve is easy and robust. *Figure 3b* and *Plate 2* show two sweep surfaces generated with the biarc method; the same axial curves in *Figure 3a* and *Plate 1* are used, respectively.

It is known[3,12] that computing an RMF on a space curve composed of piecewise plane curves is easy. For a plane curve the Frenet frame can readily be converted to an RMF by keeping the binormal at all times in a constant direction perpendicular to the embedding plane of the curve; therefore the frame given by Equation 2 is an RMF. We explore this idea by approximating an arbitrary space curve with a piecewise plane curve consisting of circular arcs. So our method is an extension of Klok's method of computing RMF[12]. We will show that, with the same number of segmentations of an axial curve, our method gives not only a better approximation of the axial curve but also a much better approximation of the RMF than Klok's method.

The circular arc has the nice property that its RMF has a simple rational parameterization as well as a simple arclength parameterization. These two parameterizations lead to a NURBS representation of the generated sweep surface and an application of our method to modeling a closed sweep surface, respectively.

A method of computing a NURBS approximation of a sweep surface generated with any moving frame has been proposed in Reference 3. However, it is assumed in that

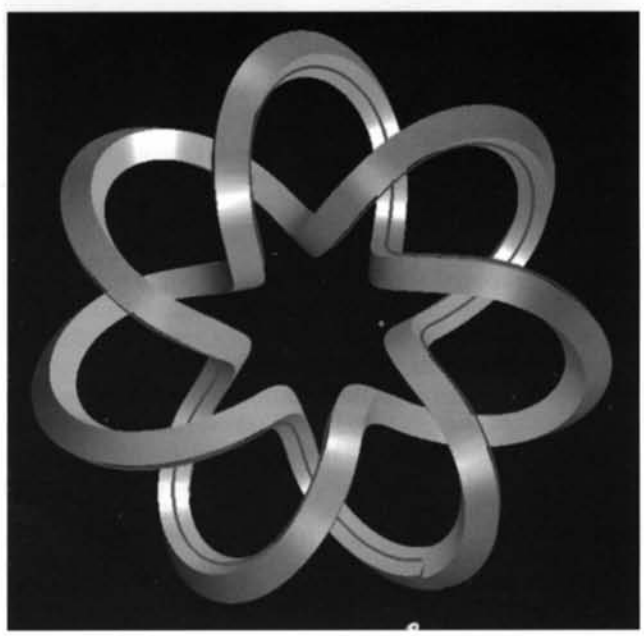

**Plate 2** A surface by the RMF computed using the biarc method, along the same torus knot

work that a moving frame has been computed before computing its NURBS approximation. Therefore the problem solved there is different from that considered in our work, as we are concerned with the robust computation and representation of the RMF, and the NURBS approximation just follows as a consequence of our algorithm.

The remainder of the paper is organized as follows. In the second and third sections we will consider using biarcs to construct a $G^1$ circular-arc spline curve to approximate the axial curve. We will also discuss the error measurement of this approximation. In the fourth section we will discuss how to compute an RMF of the circular-arc spline curve, and how to use this RMF for sweep surface modeling, including computing the NURBS representation of the sweep surface when the cross-section is a NURBS curve, and modeling a closed sweep surface when the axial curve is closed. In the fifth section we will present some examples of the sweep surfaces modeled with our method and compare our method to some other existing techniques.

## CONSTRUCTING BIARCS

The *biarc* is a space curve composed of two $G^1$ joined circular arcs. When the two arcs of a biarc are coplanar, it is called a *plane biarc*. The study of the plane biarc dates back to the 1970s[1,4,21,26]. The use of 3D biarcs in CAGD was pioneered in References 17, 20, 23. In Reference 20 the biarc is used to approximate intersection curves between two surfaces, while in References 17, 23 it is studied mainly for free-form surface modeling with cyclidal patches. A different type of circular-arc splines for fitting 3D data is discussed in Reference 11. The problem of approximating a space curve by a circular-arc spline curve has also been studied in References 20, 23. The idea is to approximate a space curve by a biarc interpolating the endpoints and end tangents of the curve.

We will give a brief review about the biarc and its construction. For more discussion on biarcs in 3D, the reader is referred to References 9, 17, 20, 23, 28. We need to list some properties of biarcs in order to derive a few new formulae for our present application. Most of these properties will be given without proofs since they can be found in the above sources.

### Properties of biarcs

Let $X_0$ and $X_1$ be two distinct points in $E^3$, represented as 3D row vectors of coordinates. Let $T_0$ and $T_1$ be unit vectors. The biarc interpolation problem is to find biarcs that interpolate the points $X_0$ and $X_1$ and have unit tangent vectors $T_0$ and $T_1$ at $X_0$ and $X_1$, respectively (see *Figure 5*). The above data for the biarc interpolation problem is denoted by $D = \{X_0, X_1, T_0, T_1\}$.

**Definition 2.1**
*Data* $D = \{X_0, X_1, T_0, T_1\}$ *is said to be* singular *if* $X_0 + \rho T_0 = X_1 + \rho T_1$ *for some* $\rho \neq 0$ *or* $T_0 = T_1$ *and* $(X_1 - X_0)T_0^T = 0$*; otherwise D is* regular.

Let a half line starting at point $X$ and going in direction $T$ be denoted by $(X,T)$. Let $\mathscr{P}$ denote the perpendicular bisecting plane of the line segment $\overline{X_0X_1}$. Then singular data $D = \{X_0, X_1, T_0, T_1\}$ is characterized by that either the half lines $(X_0, T_0)$ and $(X_1, T_1)$ intersect on the plane $\mathscr{P}$ or the half lines $(X_0, -T_0)$ and $(X_1, -T_1)$ intersect on the plane $\mathscr{P}$.

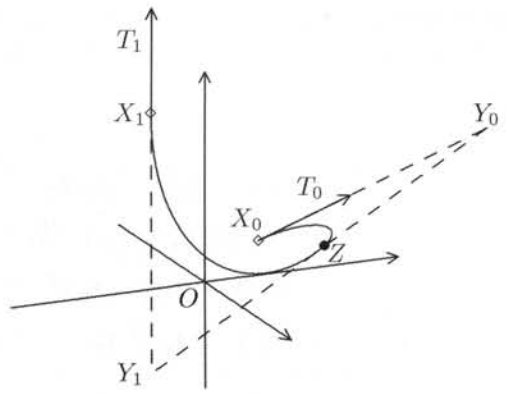


**Figure 5** A space biarc interpolating $D = \{X_0, X_1, T_0, T_1\}$

Let $B$ denote a biarc consisting of two circular arcs $C_0$ and $C_1$ joined at point $Z$, which is not necessarily a point on the curve that is being approximated. Let $\Delta X_0 Y_0 Z$ and $\Delta Z Y_1 X_1$ be the control triangles of $C_0$ and $C_1$ (see *Figure 5*). Let $Y_0 = X_0 + k_0 T_0$ and $Y_1 = X_1 - k_1 T_1$. Clearly, $k_0$ and $k_1$ are interrelated, and the pair $(k_0, k_1)$ determine a unique biarc for any given data $D$. We will assume $k_0 k_1 \neq 0$, for otherwise $C_0$ or $C_1$ degenerates into a single point and the biarc becomes degenerate.

**Property 1**[17,20,28]
*For regular data* $D = \{X_0, X_1, T_0, T_1\}$ *every solution* $(k_0, k_1)$, $k_0 k_1 \neq 0$, *of*

$$\| X_1 - X_0 \|^2 - 2k_0(X_1 - X_0)T_0^T - 2k_1(X_1 - X_0)T_1^T - 2k_0k_1(1 - T_0T_1^T) = 0 \quad (5)$$

*gives a biarc interpolating* $D = \{X_0, X_1, T_0, T_1\}$*; conversely, for any biarc interpolating D, its* $k_0$ *and* $k_1$ *satisfy Equation 5.*

Since it can be shown that Equation 5 has infinitely many solutions $(k_0, k_1)$ with $k_0 k_1 \neq 0$, there exist infinitely many biarcs interpolating data $D$. More specifically, we have the following.

**Property 2**[28]
*Let* $D = \{X_0, X_1, T_0, T_1\}$ *be regular data. When* $T_0 \neq T_1$*, the locus J of the joints of all the biarcs interpolating D is a circle passing through* $X_0$ *and* $X_1$ *(see Figure 6). The*

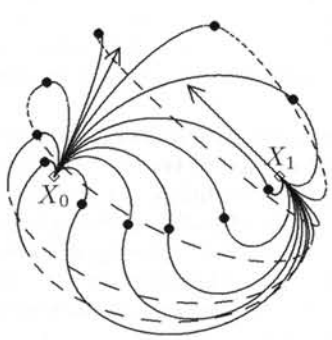


**Figure 6** The joints of the biarcs interpolating $D$ form a circle

*parametric equation of the circle J in $k_0$ is*

$$Z(k_0) = \frac{F(k_0)}{g(k_0)} \tag{6}$$

*where*

$$\begin{aligned} F(k_0) = & k_0^2\{2(1 - T_0T_1^T)X_1 + 2[(X_1 - X_0)T_0^T] \\ & \times (T_1 - T_0)\} + k_0\{2[(X_1 - X_0)T_1^T]X_1 \\ & - 2[(X_1 - X_0)T_0^T]X_0 - \| X_1 - X_0 \|^2 \\ & \times (T_1 - T_0)\} + \| X_1 - X_0 \|^2 X_0 \end{aligned}$$

*and*

$$\begin{aligned} g(k_0) = & 2k_0^2(1 - T_0T_1^T) + 2k_0(X_1 - X_0)(T_1 - T_0)^T \\ & + \| X_1 - X_0 \|^2 \end{aligned}$$

*When $T_0 = T_1$, the locus J becomes the straight line passing through $X_0$ and $X_1$.*

It was first noted in Reference 23 that all the biarcs interpolating regular data $D$ are in general contained in a sphere; they are contained in a plane when the regular data $D = \{X_0, X_1, T_0, T_1\}$ is contained in a plane. The reader is referred to Reference 9 for a geometric characterization of the circle $J$.

Suppose that the arcs $C_0$ and $C_1$ are represented as rational quadratic Bézier curves, in the form

$$Q(t) = \frac{Q_0B_{0,2}(t) + wQ_1B_{1,2}(t) + Q_2B_{2,2}(t)}{B_{0,2}(t) + wB_{1,2}(t) + B_{2,2}(t)}, \quad 0 \leqslant t \leqslant 1$$

where $B_{i,2}(t) = [2!/i!(2-i)!]t^i(1-t)^{2-i}$. By using control points at infinity, the above form can be adapted to representing a semicircle[18]. $Q(t)$ is a minor arc if $w > 0$, and a major arc if $w < 0$.

**Property 3**[28]

*For any non-zero solution $(k_0, k_1)$ of Equation 5, the weights $w_0$ and $w_1$ of the arcs $C_0$ and $C_1$ in their Bézier representations are given by*

$$w_0 = \frac{\| Z - X_0 \|}{2k_0}, \quad w_1 = \frac{\| Z - X_1 \|}{2k_1} \tag{7}$$

## Computing equal-chord biarcs

We say that $D$ is *well-behaved* if $(X_1 - X_0)T_0^T > 0$ and $(X_1 - X_0)T_1^T > 0$. The geometric meaning of well-behaved data is that the projections of $T_0$ and $T_1$ on the vector $X_1 - X_0$ are both positive, or equivalently, the angles formed by $X_1 - X_0$ with $T_0$ and $T_1$ are both less than $\pi/2$. It is easy to verify that well-behaved data are regular. We assume that all data $D$ considered from now on are well-behaved.

By Property 3, the arcs $C_0$ and $C_1$ of a biarc are minor arcs if and only if $k_0 > 0$ and $k_1 > 0$. Since minor arcs have relatively small windings as compared with major arcs, they are more desirable than major arcs for shape design. We now consider choosing a biarc interpolating $D$ that always consists of two minor arcs. The two arcs of the biarc we will choose have equal-length chords, so it is called *the equal-chord biarc*.

The use of equal-chord biarcs is first suggested in References 9, 23, but only in geometric terms. So we will derive some formulae necessary for computing the equal-chord biarc. To determine the joint of the equal-chord biarc, we use the perpendicular bisecting plane of the line segment $\overline{X_0X_1}$ to intersect the circle $J$, the locus of biarc joints (see Property 2). The equation of this plane is

$$(2X - X_0 - X_1)(X_1 - X_0)^T = 0$$

Substituting the parametric Equation 6 of $J$ into the above equation, we obtain a quadratic equation in $k_0$,

$$ak_0^2 + bk_0 + c = 0 \tag{8}$$

where

$$\begin{aligned} a = & 2 \| X_1 - X_0 \|^2 (1 - T_0T_1^T) + 4[(X_1 - X_0)T_0^T] \\ & \times [(X_1 - X_0)(T_1 - T_0)^T] \\ b = & 4[(X_1 - X_0)T_0^T] \| X_1 - X_0 \|^2 \\ c = & - \| X_1 - X_0 \|^4 \end{aligned}$$

Geometrically, it is obvious that there are two intersections between the plane and the circle $J$. Algebraically, after simplification, we have the determinant

$$\begin{aligned} \Delta = & 4 \| X_1 - X_0 \|^4 \{4[(X_1 - X_0)T_0^T][(X_1 - X_0)T_1^T] \\ & + \| T_1 - T_0 \|^2 \| X_1 - X_0 \|^2\} \\ \geqslant & 4 \| X_0 - X_1 \|^4 \{4[(X_1 - X_0)T_0^T][(X_1 - X_0)T_1^T] \\ & + [(X_1 - X_0)(T_1 - T_0)^T]^2\} \\ = & 4 \| X_1 - X_0 \|^4 [(X_1 - X_0)(T_1 + T_0)^T]^2 > 0 \end{aligned}$$

The first inequality is by Cauchy–Schwarz inequality, and the second inequality follows from the assumption that $D$ is well-behaved.

Let $H = \Delta/(4 \| X_1 - X_0 \|^4)$. Then $H > 0$. After simplification, the two solutions of $k_0$ from Equation 8, together with their corresponding $k_1$ solved from Equation 5, can be shown to be

$$k_0^{(1)} = \frac{\| X_1 - X_0 \|^2}{2(X_1 - X_0)T_0^T + \sqrt{H}}$$

$$k_1^{(1)} = \frac{\| X_1 - X_0 \|^2}{2(X_1 - X_0)T_1^T + \sqrt{H}}$$

and

$$k_0^{(2)} = \frac{\| X_1 - X_0 \|^2}{2(X_1 - X_0)T_0^T - \sqrt{H}}$$

$$k_1^{(2)} = \frac{\| X_1 - X_0 \|^2}{2(X_1 - X_0)T_1^T - \sqrt{H}}$$

Thus there are two equal-chord biarcs, given by these two pairs of solutions. Since the solution pair $(k_0^{(1)}, k_1^{(1)})$ are always positive for any well-behaved data, meaning that the corresponding equal-chord biarc always consists of two minor arcs, we will choose the biarc given by $(k_0^{(1)}, k_1^{(1)})$ and call it *the* equal-chord biarc.

There have been other choices of the biarc proposed in the literature, such as the biarc with $k_0 = k_1 > 0$ in Reference 20 and the minimum twist biarc in Reference 17. It is shown empirically in Reference 27 that in most cases the equal-chord biarc has the smallest difference

between the curvature radii of the two arcs than that of the biarcs given by the other two choices. This is another reason why the equal-chord biarc is used in this work.

## APPROXIMATING AXIAL CURVES

### Adaptive subdivision and approximation

In this section we consider constructing a $G^1$ circular-arc spline curve to approximate the given axial curve $A(u)$. The curve $A(u)$ is first subdivided into short curve segments whose endpoints $X_0, X_1$ and end tangent directions $T_0, T_1$ form well-behaved data. Each curve segment is then approximated by an equal-chord biarc. In the following we will emphasize on the error estimation of this approximation.

In many applications it is required that the error of approximation be less then a prescribed tolerance $\epsilon$. This requirement can be met by adaptively subdividing the axial curve $A(u)$. Let $P(u), u_0 \leqslant u \leqslant u_1$, be a curve segment resulting from an initial subdivision of $A(u)$. Let $X_0 = P(u_0)$, $X_1 = P(u_1)$, $T_0 = P'(u_0)/\parallel P'(u_0) \parallel$, and $T_1 = P'(u_1)/\parallel P'(u_1) \parallel$. Then $P(u)$ is approximated by the equal-chord biarc $B$ interpolating $D = \{X_0, X_1, T_0, T_1\}$. Assume for the moment that an estimate $\delta$ of the approximation error of $P(u)$ by $B$ can be obtained. If $\delta \leqslant \epsilon$, the approximation will be accepted; otherwise $P(u)$ will be further subdivided into two pieces, $P_0(u) = P(u)$, $u_0 \leqslant u \leqslant (u_0 + u_1)/2$, and $P_1(u) = P(u)$, $(u_0 + u_1)/2 \leqslant u \leqslant u_1$. $P_0(u)$ and $P_1(u)$ are then approximated by the equal-chord biarcs respectively, and the error analysis is performed for each piece again. Error estimation and subdivision are repeated recursively until the error tolerance is satisfied over all the curve segments resulting from subdividing $A(u)$. We assume that all the above interpolation data are well-behaved.

It has been proved[29] that the above approximation process is convergent and the approximation error of the equal-chord biarc is $O(h^3)$, where $h$ is the arclength of the curve segment approximated by the biarc. This means that subdividing a curve segment into two pieces of about equal length reduces the approximation error asymptotically by a factor of 8. For a study of this problem in the setting of approximating a planar curve by plane biarcs, the reader is referred to Reference 16.

### Error estimation

In the approximation procedure above we still need to compute a tight estimate of the approximation error to decide whether or not the prescribed error tolerance is satisfied. The approximation error is the distance between the curve approximated and the circular-arc spline curve. Measuring the distance between two space curves is different from and more difficult than measuring the 'distance' between two univariate functions. A simple approach is to sample a set of points on the biarc and another set of points on the curve segment approximated, and then compute the Hausdorff distance $d_H(\cdot, \cdot)$ between the two sets. The distance $d_H(\cdot, \cdot)$ is defined as

$$d_H(A, B) = \max\{\max_x \min_y \{d(x, y) | x \in A, y \in B\},$$

$$\max_y \min_x \{d(x, y) | x \in A, y \in B\}\}$$

for two compact sets of $A$ and $B$ of $E^3$, where $d(\cdot, \cdot)$ is the Euclidean distance between two points. Although this approach works for any two parametric curves in space, besides being computationally expensive, it is difficult to use because choosing an effective sampling interval depends very much on the distance to be measured.

We describe an efficient method that computes accurately the approximation error at any point of a parametric curve $A(u)$ approximated by a biarc. Thus computing the error is reduced to evaluating a univariate function $d(u)$ defined on the curve. We also consider obtaining an upper bound of the approximation error when $A(u)$ is a rational curve.

To simplify discussion, we make the practical assumption that the approximation of the original axial curve by the biarc spline curve is fine enough so that the normal plane at any point of the biarc spline curve intersects the approximated axial curve in exactly one point in a neighborhood of the biarc spline curve.

Let $R(u), u \in [u_0, u_1]$, be a curve segment on the axial curve $A(u)$. Suppose $R(u)$ is approximated by an equal-chord biarc $B$ consisting of two arcs $C_0$ and $C_1$. The segment $R(u)$ is first subdivided into two segments $R_0(u)$ and $R_1(u)$ by the normal plane $V$ of the biarc $B$ at the joint of its two arcs. Then the distance from $R_0(u)$ to $C_0$ and the distance from $R_1(u)$ to $C_1$ are computed.

Now we have reduced the problem to computing the distance from a parametric curve to a single circular arc. Since a circle in $E^3$ is the intersection of a plane and a right circular cylinder, the problem is further reduced to computing the distance from a parametric curve to the plane and the cylinder (see *Figure 7*).

Suppose the curve $P(u), u \in [0, 1]$, is approximated by circular arc $C$ in space. Let $N$ be the unit normal vector of the plane containing the arc $C$. Let $O_C$ be the center of the arc $C$, and $r$ be the radius of $C$. Then the circle containing $C$ is the intersection of the plane $f(X) \equiv (X - O_C)N^T = 0$ and the right circular cylinder $g(X) \equiv \parallel (X - O_C) - [(X - O_C)N^T]N \parallel - r = 0$, where $X = (x, y, z)$, and $\parallel . \parallel$ is Euclidean norm. Then $|f(X)|$ and $|g(X)|$ are the distances of a point $X$ to the plane and the cylinder, respectively (see *Figure 7*). The distance from point $P(u)$ to the circle containing $C$ is therefore

$$d(u) = [f^2(P(u)) + g^2(P(u))]^{1/2}, \quad u \in [0, 1]$$

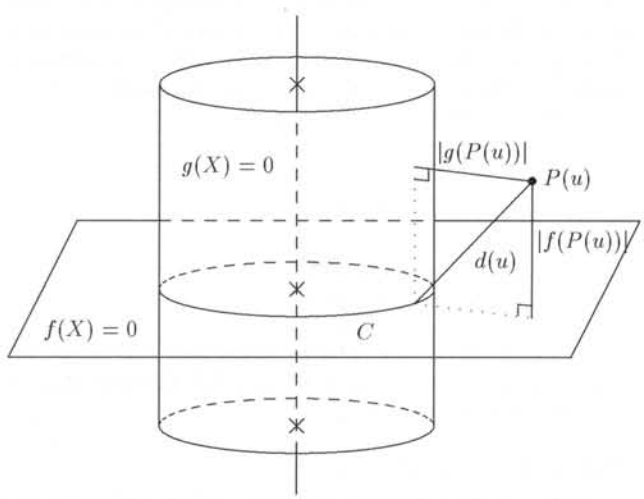


**Figure 7** Distance measurement from $P(u)$ to circular arc $C$

From the assumption that approximation by the biarc spline curve is fine enough, and because we always use the normal plane of the biarc at its joint to subdivide the curve approximated into two parts, the whole curve $P(u)$ lies in the wedge of the cylinder subtended by the arc $C$. So $d(u)$ is also the distance from the point $P(u)$ to the arc $C$.

The maximum error over the whole curve $P(u)$ is then

$$d_P = \max_{u\in[0,1]} d(u) = \max_{u\in[0,1]} [f^2(P(u)) + g^2(P(u))]^{1/2} \quad (9)$$

Using Equation 9, $d_P$ can be approximated by evaluating $d(u)$ at a sufficient number of values of $u$.

When $P(u)$ is a rational curve, it is possible to obtain an upper bound of $d_P$ that is easy to compute. Since

$$\max_{u\in[0,1]} [f^2(P(u)) + g^2(P(u))]^{1/2} \leqslant \max_{u\in[0,1]} |f(P(u))| + \max_{u\in[0,1]} |g(P(u))|$$

we have

$$\bar{d}_P = \max_{u\in[0,1]} |f(P(u))| + \max_{u\in[0,1]} |g(P(u))|$$

as an upper bound of $d_P$. Let $h(X) = (\| (X - O_C) \|^2 - [(X - O_C)N^T]^2 - r^2)/r$. As

$$|g(X)| = \left| \frac{\| (X - O_C) - [(X - O_C)N^T]N \|^2 - r^2}{\| (X - O_C) - [(X - O_C)N^T]N \| + r} \right| \leqslant \left| \frac{\| (X - O_C) - [(X - O_C)N^T]N \|^2 - r^2}{r} \right| = \left| \frac{\| (X - O_C) \|^2 - [(X - O_C)N^T]^2 - r^2}{r} \right| = |h(X)|$$

$$\tilde{d}_P = \max_{u\in[0,1]} |f(P(u))| + \max_{u\in[0,1]} |h(P(u))|$$

is an upper bound of $d_P$ since $\tilde{d}_P \geqslant \bar{d}_P$. Let the Bézier representation of $P(u)$ be

$$P(u) = \frac{\sum_{i=0}^{k} w_i P_i B_{i,k}(u)}{\sum_{i=0}^{k} w_i B_{i,k}(u)}, \quad u \in [0, 1]$$

We may assume that all the weights $w_i$ of $P(u)$ are non-negative, as any finite and continuous piece of a rational curve can be subdivided into sufficiently short segments which have a Bézier representation with non-negative weights[14]. Then, representing the polynomials $f(P(u))$ and $h(P(u))$ in Bernstein basis, we have

$$f(P(u)) = \frac{\sum_{i=0}^{k} w_i^f f_i B_{i,k}(u)}{\sum_{i=0}^{k} w_i^f B_{i,k}(u)}$$

$$h(P(u)) = \frac{\sum_{i=0}^{2k} w_i^h h_i B_{i,2k}(u)}{\sum_{i=0}^{2k} w_i^h B_{i,2k}(u)}$$

with the weights $w_i^f = w_i$ and $w_i^h$ being also non-negative. Denote $D_{\max} = \max_{i=0}^{k} |f_i| + \max_{i=0}^{2k} |h_i|$. Clearly $D_{\max}$ is an upper bound of $d_P$, as

$$D_{\max} \geqslant \tilde{d}_P \geqslant \bar{d}_P \geqslant d_P$$

It can be shown, though less trivially, that $D_{\max}$ is less than a constant multiple of $d_P$; but we will not pursue these details here. Our experience shows that, asymptotically, $D_{\max} \leqslant 4d_P$ when $P(u)$ is a cubic polynomial curve.

**Example 3.1**
Consider the cubic Bézier curve $P(u)$,

$$P(u) = P_0 B_{0,3}(u) + P_1 B_{1,3}(u) + P_2 B_{2,3}(u) + P_3 B_{3,3}(u), \quad 0 \leqslant u \leqslant 1 \quad (10)$$

where $P_0 = [0.0, 0.0, -0.75]$, $P_1 = [2.0, 0.0, -0.25]$, $P_2 = [0.0, 2.0, 0.25]$, and $P_3 = [0.0, 0.0, 0.75]$. The curve is subdivided into $2^d$ segments in $d$ levels of binary subdivision, $1 \leqslant d \leqslant 11$, so at level $d$, $2^d$ biarcs are used to approximate $P(u)$. The approximation errors at all the levels are listed in *Table 1*. It can be seen that, as expected, the approximation error decreases by a factor of about 8 with each subdivision.

## GENERATING SWEEP SURFACE

Let $\mathscr{C}$ denote the circular-arc spline curve approximating the axial curve $A(u)$. We now compute a rotation minimizing frame (RMF) of $\mathscr{C}$ to generate a sweep surface along $\mathscr{C}$. To this end we need to assign a parameterization to $\mathscr{C}$. In the following we will discuss the rational quadratic parameterization and the arclength parameterization of $\mathscr{C}$.

### Rational quadratic parameterization

#### Representing RMF in NURBS form

Suppose that $\mathscr{C}$ is composed of $n$ circular arcs. Since a circular arc is a rational quadratic Bézier curve, $\mathscr{C}$ is a quadratic NURBS curve with double knots. Let a circular arc of $\mathscr{C}$ be

$$Q(t) = \frac{Q_0 B_{0,2}(t) + w_1 Q_1 B_{1,2}(t) + Q_2 B_{2,2}(t)}{w(t)}, \quad t \in [0, 1]$$

where $w(t) = B_{0,2}(t) + w_1 B_{1,2}(t) + B_{2,2}(t)$. We now compute the Frenet frame $F(t) = [X(t)\ Y(t)\ Z(t)]$ of $Q(t)$, which is also an RMF of $Q(t)$. Assume for the moment that $Q(t)$ is not a straight line segment. Let $O$ be the center and $r$ the radius of the underlying circle of the arc $Q(t)$. Let $X_j = (O - Q_j)/r$, $j = 0, 1, 2$. Then the unit

**Table 1** The error of approximation of a cubic curve (Equation 10) by $n = 2^d$ space biarcs

| Depth of subdivision ($d$) | Error |
|---|---|
| 1 | $7.31 \times 10^{-2}$ |
| 2 | $1.47 \times 10^{-2}$ |
| 3 | $1.68 \times 10^{-3}$ |
| 4 | $1.48 \times 10^{-4}$ |
| 5 | $1.54 \times 10^{-5}$ |
| 6 | $1.72 \times 10^{-6}$ |
| 7 | $2.02 \times 10^{-7}$ |
| 8 | $2.45 \times 10^{-8}$ |
| 9 | $3.03 \times 10^{-9}$ |
| 10 | $3.76 \times 10^{-10}$ |
| 11 | $4.70 \times 10^{-11}$ |

normal vector of $Q(t)$ is

$$X(t) = \frac{O - Q(t)}{r} = \frac{X_0 B_{0,2}(t) + w_1 X_1 B_{1,2}(t) + X_2 B_{2,2}(t)}{w(t)}$$

Let $N_0$ denote the unit normal vector of the plane containing $Q(t)$. Then

$$N_0 = \frac{(Q_1 - Q_0) \times (Q_2 - Q_0)}{\| (Q_1 - Q_0) \times (Q_2 - Q_0) \|}$$

Let $Y(t) = N_0$. Then

$$Y(t) = \frac{Y_0 B_{0,2}(t) + w_1 Y_1 B_{1,2}(t) + Y_2 B_{2,2}(t)}{w(t)}$$

where $Y_0 = Y_1 = Y_2 = N_0$. Denoting $Z_j = X_j \times Y_j$, $j = 0, 1, 2$, the unit tangent vector of $Q(t)$ is

$$Z(t) = X(t) \times Y(t) = \frac{Z_0 B_{0,2}(t) + w_1 Z_1 B_{1,2}(t) + Z_2 B_{2,2}(t)}{w(t)}$$

Therefore the Frenet frame is

$$\begin{aligned} F(t) &= [X(t)\ Y(t)\ Z(t)] \\ &= \frac{1}{w(t)} \{ [X_0\ Y_0\ Z_0] B_{0,2}(t) + w_1 [X_1\ Y_1\ Z_1] B_{1,2}(t) \\ &\quad + [X_2\ Y_2\ Z_2] B_{2,2}(t) \} \\ &= \frac{F_0 B_{0,2}(t) + w_1 F_1 B_{1,2}(t) + F_2 B_{2,2}(t)}{B_{0,2}(t) + w_1 B_{1,2}(t) + B_{2,2}(t)} \end{aligned} \tag{11}$$

where $F_j = [X_j\ Y_j\ Z_j]$, $j = 0, 1, 2$.

Let $F_i(t)$ denote the Frenet frame of the $i$th arc $Q_i(t)$ of $\mathscr{C}$. Denote

$$F_i(t) = \frac{F_{i,0} B_{0,2}(t) + w_{i,1} F_{i,1} B_{1,2}(t) + F_{i,2} B_{2,2}(t)}{B_{0,2}(t) + w_{i,1} B_{1,2}(t) + B_{2,2}(t)}, \quad i = 0, 1, \ldots n-1 \tag{12}$$

Because two adjacent circular arcs $Q_i(t)$ and $Q_{i+1}(t)$ of $\mathscr{C}$ are in general not coplanar, $F_i(t)$ and $F_{i+1}(t)$ are discontinuous at the joining point (see *Figure 8*).

In this case the angle between the normal vectors of $Q_i(t)$ and $Q_{i+1}(t)$ at their joint should be used to adjust the subsequent frame so that the two frames meet continuously at the joint.

Specifically, let $\theta_{i+1}$ be the angle between the normal vector $X_i(1)$ of the arc $Q_i(t)$ and the normal vector $X_{i+1}(0)$ of the arc $Q_{i+1}(t)$, which is defined by

$$\theta_{i+1} = \text{sign}[(X_{i+1}(0) \times X_i(1)) Z_i(1)^T] \times \arccos[X_i(1) X_{i+1}(0)^T]$$

Define

$$\alpha_{i+1} = \alpha_i + \theta_{i+1}, \quad i = 0, 1, \ldots, n-2$$

with $\alpha_0$ being a user-specified constant. Then a continuous RMF of $\mathscr{C}$ is defined by a sequence of frames $G_i(t)$ over the arcs $Q_i(t)$, and the $G_i(t)$ are obtained by adjusting the $F_i(t)$ as follows,

$$G_i(t) = F_i(t) R_Z(\alpha_i), \quad i = 0, 1, \ldots, n-1$$

where $R_Z(\alpha)$ is a rotation of angle $\alpha$ about the $Z$-axis.

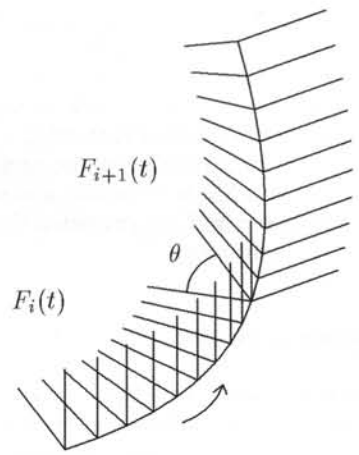


**Figure 8** Discontinuity between two consecutive frames

So, by Equation 12,

$$G_i(t) = \frac{G_{i,0} B_{0,2}(t) + w_{i,1} G_{i,1} B_{1,2}(t) + G_{i,2} B_{2,2}(t)}{B_{0,2}(t) + w_{i,1} B_{1,2}(t) + B_{2,2}(t)}, \quad i = 0, 1, \ldots, n-1 \tag{13}$$

where $G_{i,j} = F_{i,j} R_Z(\alpha_i)$, $j = 0, 1, 2$.

It has been assumed so far that each $Q_i(t)$ is a circular arc with a finite radius. When $Q_i(t)$ is a line segment, its center and radius are not defined, neither are the vectors $X_i(t)$ and $Y_i(t)$. In this case the frame $G_i(t)$ should be defined as a constant frame equal to the ending frame of the preceding arc (see *Figure 9*).

**NURBS sweep surfaces**

Since the RMF of the axial curve $\mathscr{C}$ has rational parameterization, when the cross-section is given as a NURBS curve, the sweep surface generated along $\mathscr{C}$ is representable as a NURBS surface. We now give the expression for this NURBS sweep surface. Let the cross-section curve be

$$C(v) = \frac{\sum_{k=0}^{p} g_k C_k N_{k,l}(v)}{\sum_{k=0}^{p} g_k N_{k,l}(v)} \tag{14}$$

By Equations 13 and 14, the sweep surface patch over the arc $Q_i(t)$ is

$$\begin{aligned} S_i(t, v) &= G_i(t) C(v) + Q_i(t) \\ &= \frac{\sum_{j=0}^{2} \sum_{k=0}^{p} w_{i,j} g_k (G_{i,j} C_k + Q_{i,j}) B_{j,2}(t) N_{k,l}(v)}{\sum_{j=0}^{2} \sum_{k=0}^{p} w_{i,j} g_k B_{j,2}(t) N_{k,l}(v)}, \\ &\quad t \in [0, 1],\ i = 0, 1, 2, \ldots, n-1 \end{aligned}$$

where $w_{i,0} = w_{i,2} = 1$. The collection of the $S_i(t, v)$ is

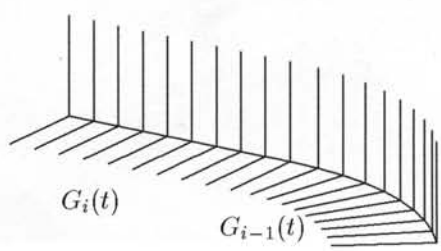


**Figure 9** An RMF on a line segment

expediently denoted by $S(t, v)$. A NURBS sweep surface thus generated is shown in *Figure 10*.

Since the frames $G_i(t)$ are continuous along $\mathscr{C}$, the patches $S_i(t, v)$ are continuous along $\mathscr{C}$ as well. Furthermore, because the partial derivatives $\partial S_i(t, v)/\partial t|_{t=1}$ and $\partial S_{i+1}(t, v)/\partial t_{t=0}$ are both parallel to the vector $Q_i'(t)|_{t=1}$, the patches $S_i(t, v)$ and $S_{i+1}(t, v)$ in fact join with $G^1$ continuity across the curve $S_i(1, v)$, provided that the cross-section $C(v)$ is $G^1$ continuous.

## Arclength parameterization

### Arclength parameterization of RMF

Circular arcs have simple arclength parameterizations in terms of trigonometric functions. Assume that all the arcs of $\mathscr{C}$ are minor arcs and are not straight line segments. Suppose that the $i$th arc of $\mathscr{C}$ has endpoints $P_{i,0}$ and $P_{i,1}$, center $O_i$, radius $r_i$, and arclength $s_i$. Then this arc has the arclength parameterization

$$P_i(s) = O_i + \frac{(P_{i,0} - O_i)\sin(\theta_i - s/r_i) + (P_{i,1} - O_i)\sin(s/r_i)}{\sin\theta_i}, \quad s \in [0, s_i]$$

where $\theta_i$ is the central angle subtended by the arc $P_i(s)$, and $O < \theta_i < \pi$ by assumption. To our knowledge this nice expression for the arclength parameterization of a circular arc appeared first in Reference 24, though in a slightly different form.

Let the Frenet frame of $P_i(s)$ (also an RMF in this case) be $F_i(s) = [X_i(s)\ Y_i(s)\ Z_i(s)]$. Then it is easy to show that

$$X_i(s) = \frac{X_{i,0}\sin(\theta_i - s/r_i) + X_{i,1}\sin(s/r_i)}{\sin\theta_i}$$

$$Y_i(s) = \frac{(P_{i,0} - O_i) \times (P_{i,1} - O_i)}{\| (P_{i,0} - O_i) \times (P_{i,1} - O_i) \|} \equiv Y_i$$

$$Z_i(s) = X_i(s) \times Y_i(s) = \frac{Z_{i,0}\sin(\theta_i - s/r_i) + Z_{i,1}\sin(s/r_i)}{\sin\theta_i}, \quad s \in [0, s_i]$$

where

$$X_{i,j} = (O_i - P_{i,j})/r_i \text{ and } Z_{i,j} = X_{i,j} \times Y_{i,j} = 0, 1$$

Similar to the case of rational quadratic parameterization, the frames $F_i(s)$ can be adjusted to form a continuous RMF of $\mathscr{C}$, which can then be used to generate a $G^1$ sweep surface along $\mathscr{C}$. We will not repeat the details here.

### Modeling closed sweep surface

The advantage of parameterizing $\mathscr{C}$ in arclength is that one can sample points of $\mathscr{C}$ evenly with respect to arclength. Here we discuss an application of the arclength parameterization of RMF to modeling *a closed sweep surface*; that is, the axial curve is given as a closed smooth space curve and it is required that the sweep surface be also closed and smooth. Note that the RMF of a closed smooth axial curve does not in general result in a closed sweep surface. So we have to adjust the RMF of $\mathscr{C}$ into such a moving frame that the generated sweep surface is closed and, meanwhile, the new moving frame deviates from the RMF as little as possible.

Any moving frame of the axial curve $\mathscr{C}$ can be obtained by twisting the RMF of $\mathscr{C}$ about the tangent of $\mathscr{C}$. With the arclength parametrization of $\mathscr{C}$, all we need to do is sample the RMF of $\mathscr{C}$ with equal arclength intervals and evenly distribute the amount of twist of the new moving frame by arclength along $\mathscr{C}$. This task is facilitated by the simple arclength parameterization of $\mathscr{C}$. Three closed sweep surfaces modeled using this method are shown in *Plates 3–5*.

Let a smooth and closed axial curve $\mathscr{C}$ be denoted by $P(t)$, $t \in [0, 1]$, i.e. $P(0) = P(1)$ and $P'(0)/\| P'(0) \| = P'(1)/\| P'(1) \|$. When a global twist is required to make the two ends of the sweep surface meet smoothly,

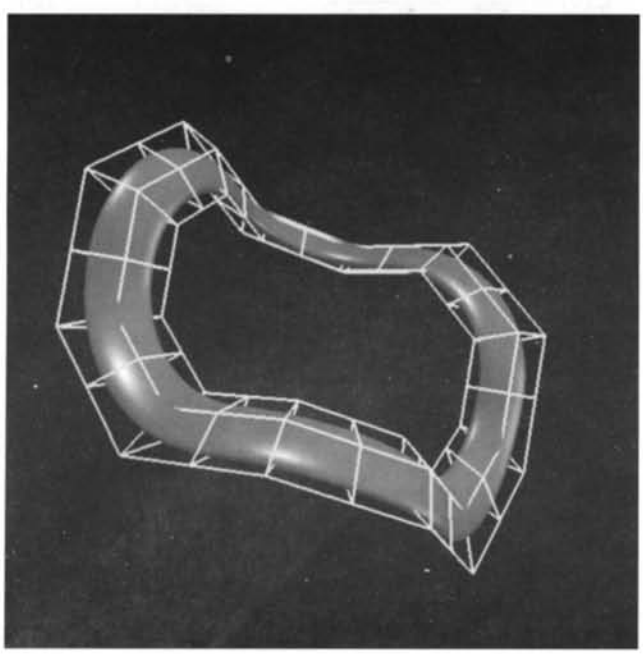

**Figure 10** A NURBS sweep surface generated by the biarc method

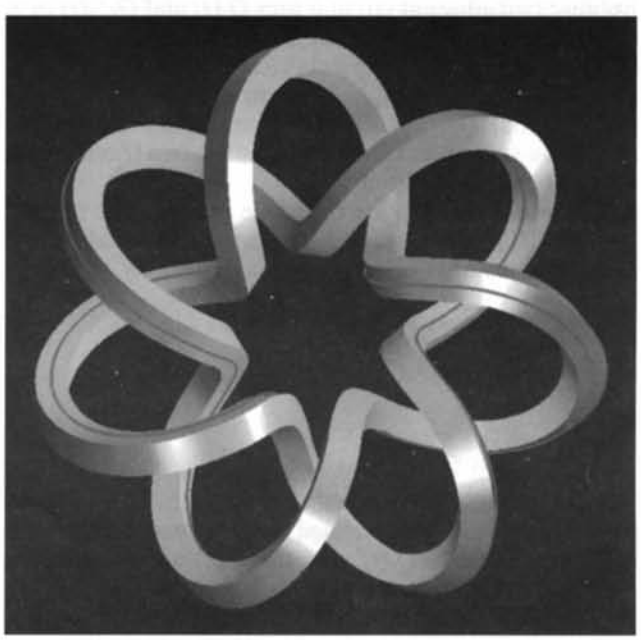

**Plate 3** A closed surface given by the biarc method, along the same torus knot

**Plate 4** A closed surface computed using the biarc method

assuming that the twist is evenly distributed over the parameter domain $t \in [0, 1]$, a sufficient and necessary condition for the sweep surface to be smooth at the end is that $P'(0) = P'(1)$. The arclength parameterization meets this condition and, in addition, allows uniform distribution of the twist along the axial curve.

## DISCUSSIONS

### Examples

A set of examples are first given to show the difference between the biarc method and two other methods for computing a moving frame along a free-form curve.

**Example 1**
*Figure 11a–d* shows four sweep surfaces generated with the same cross-section curve and closed axial curve. *Figure 11a* is by the RMF computed by the biarc method; it is a NURBS surface and not closed. *Figure 11b* is the closed sweep surface computed by the biarc method with twist adjustment; it is not a NURBS surface. *Figure 11c* is by the Frenet frame defined by Equation 1; it is a closed surface. *Figure 11d* is by the RMF computed by numerically integrating Equation 4. Note that the Frenet frame and the RMF computed by numerically integrating Equation 4 fail to produce a smooth surface, as explained in the Introduction.

**Example 2**
The biarc method has circular arc precision; that is, if the given axial curve is a circle, then it is accurately reproduced by the biarc approximation. *Plate 6* shows a torus in NURBS form which is accurately modeled by the biarc method.

### Comparisons

The method based on the integral formula[10] works well for an axial curve $A(u)$ that is $C^3$ with $A'(u) \times A''(u) \neq 0$, but fails for a regular and smooth curve with $A'(u) \times A''(u) = 0$ at some points. By contrast, our method is robust and is applicable to any regular space curve. This is illustrated by *Figures 1b* and *c*, and also by *Figures 11a* and *d*.

We use a helix as the axial curve to compare the approximation errors of the RMFs given by the biarc method and Klok's linear approximation method. The helix is given by $P(t) = (0.3\sin(t), 0.3\cos(t), 0.5t)$, $t \in [0, 2\pi]$. Suppose the initial frame of the RMF of the helix is the same as the initial frame of the Frenet frame at the starting point $P(0)$ of the helix. It can be calculated by Equation 4 that the angle difference between the RMF and the Frenet frame at the

**Plate 5** A Mobius strip generated by the biarc method using twist adjustment

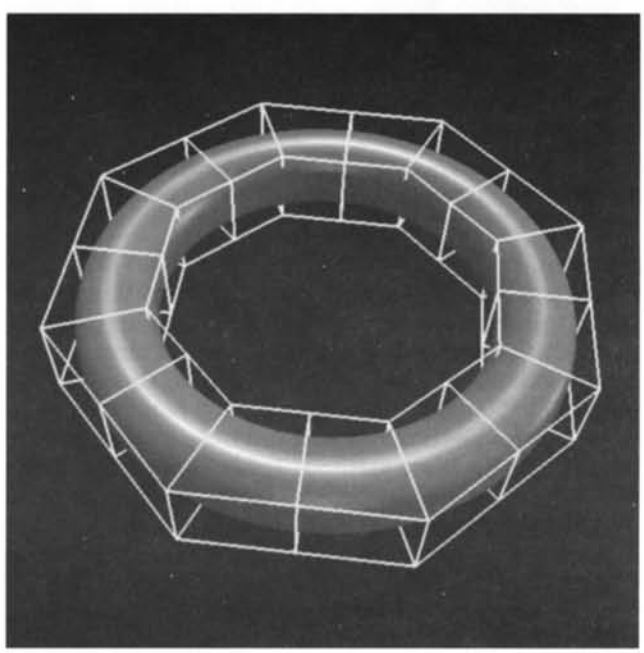

**Plate 6** A torus in NURBS representation generated accurately by the biarc method

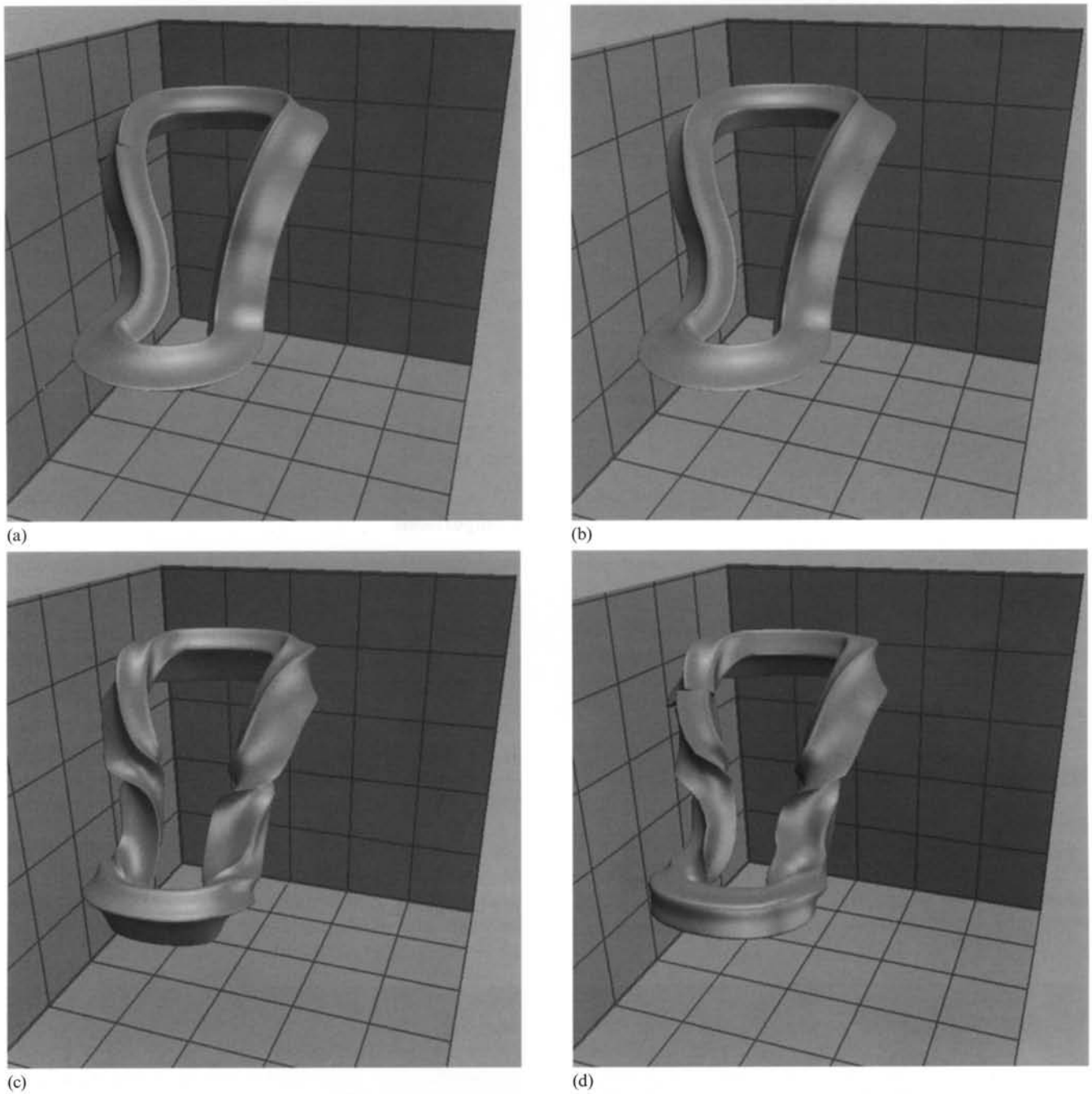

**Figure 11** (a) A surface generated by the RMF computed using the biarc method. (b) A closed surface generated using the biarc method. (c) A surface generated by the Frenet frame. (d) A surface generated by the RMF computed according to Equation 4

endpoint $P(2\pi)$ of the helix is $\Theta = 5.387782$. It is found that, to approximate the RMF to within 1% of $\Theta$, 12 segments are required by the linear approximation method and only 4 segments are required by the biarc method. Further, to approximate the RMF to within 0.01% of $\Theta$, 119 segments are required by the linear approximation method and only 9 segments are required by the biarc method. *Table 2* shows the errors of RMFs computed by the two methods with the same number of segments, $n$. It is found empirically that, for a general axial curve of finite length, the approximation error of the RMF by the biarc method is $O(n^{-4})$, and the error by the linear approximation method is $O(n^{-2})$. Thus the biarc method is much more effective than the linear approximation method in approximating the RMF.

## Conclusion

Both the polygonal approximation method by Klok[12] and the biarc method compute robustly an RMF along a smooth axial curve for sweep surface modeling. The biarc method has several advantages over the polygonal method:

(1) The biarc method yields the same approximation error of a general axial curve with fewer number of segments than the polygonal approximation method would require. [The error of the approximation to the axial curve is $O(h^2)$ for Klok's method vs $O(h^3)$ for the biarc method.]
(2) The biarc method yields the same approximation error of the RMF of a general axial curve with fewer

**Table 2** The approximation errors of RMF by the biarc method and the linear approximation method

| $n$ No. of segments | Error of biarc method | Error of linear method |
|---|---|---|
| 4 | $8.46 \times 10^{-3}$ | $2.89 \times 10^{-1}$ |
| 8 | $5.47 \times 10^{-4}$ | $9.52 \times 10^{-2}$ |
| 16 | $3.45 \times 10^{-5}$ | $2.73 \times 10^{-2}$ |
| 32 | $2.16 \times 10^{-6}$ | $7.19 \times 10^{-3}$ |
| 64 | $1.35 \times 10^{-7}$ | $1.84 \times 10^{-3}$ |
| 128 | $8.46 \times 10^{-9}$ | $4.64 \times 10^{-4}$ |
| 256 | $5.29 \times 10^{-10}$ | $1.17 \times 10^{-4}$ |
| 512 | $3.31 \times 10^{-11}$ | $2.92 \times 10^{-5}$ |

number of segments than the polygonal approximation method would require. [The error of the approximation to the RMF is $O(n^{-2})$ for Klok's method vs $O(n^{-4})$ for the biarc method.]

(3) The approximate sweep surface produced by the biarc method is $G^1$ smooth and is in NURBS form, provided that the cross-section is a NURBS curve. So the representation is rendering-resolution independent and can be used as an internal representation of the sweep surface for further surface editing.

## ACKNOWLEDGEMENTS

The authors are grateful to the referees for their helpful comments that improved the presentation of this paper.

## REFERENCES

1. Bézier, P., *Numerical Control*. Wiley, London, 1972.
2. Bishop, R. L., There is more than one way to frame a curve. *American Mathematical Monthly*, 1975, **82,** 246–251.
3. Bloomenthal, M. and Riesenfeld, R. F., Approximation of sweep surfaces by tensor product NURBS. *SPIE Proceedings: Curves and Surfaces in Computer Vision and Graphics II*, vol. 1610, ed. M. J. Silbermann and H. D. Tagare, 1991, pp. 132–154.
4. Bolton, K. M., Biarc curves. *Computer-Aided Design*, 1975, **7**(2), 89–92.
5. Bronsvoort, W., A. surface-scanning algorithm for displaying generalized cylinders. *The Visual Computer*, 1992, **8**(3), 162–170.
6. Bronsvoort, W. and Klok, F., Ray tracing generalized cylinders. *ACM Transactions on Graphics*, 1985, **4**(4), pp. 291–303.
7. Chung, T. L. and Wang, W., Discrete moving frames for sweep surface modeling. To appear in *Proceedings of Pacific Graphics '96*, 1996, pp. 159–172.
8. Coquillart, S., A control-point-based sweeping technique. *IEEE CG&A*, 1987, **7**(11), 36–45.
9. Fuhs, W. and Stachel, H., Circular pipe-connections. *Computer & Graphics*, 1988, **12**(1), 53–57.
10. Guggenheimer, H. W., Computing frames along a trajectory. *Computer Aided Geometric Design*, 1989, **6,** 77–78.
11. Hoschek, J., Circular splines. *Computer-Aided Design*, 1992, **24**(11), 611–618.
12. Klok, F., Two moving coordinate frames for sweeping along a 3D trajectory. *Computer Aided Geometric Design*, 1986, **3,** 217–229.
13. Kreyszig, E., *Differential Geometry*. The University of Toronto Press, Toronto, 1963.
14. Lane, J. and Riesenfeld, R., A theoretical development for the computer generation and display of piecewise polynomial surfaces. *IEEE Trans. PAMI*, 1980, **2,** 35–46.
15. Manocha, D. and Canny, J. F., Detection cusps and inflection points in curves. *Computer Aided Geometric Design*, 1992, **9,** 1–24.
16. Meek, D. S. and Walton, D. J., Approximating smooth planar curves by arc splines. *Journal of Computational and Applied Mathematics*, 1995, **59,** 221–231.
17. Nutbourne, A. W. and Martin, R. R., *Differential Geometry Applied to Curve and Surface Design, Vol 1: Foundations*. Ellis Horwood, England, 1988.
18. Piegl, L., Infinite control points—a method for representing surfaces of revolution using boundary data. *IEEE CG&A*, 1987, March, 45–55.
19. Piegl, L. and Tiller, W., *The NURBS Book*. Springer, 1995.
20. Rossignac, J. R. and Requicha, A. A., Piecewise-circular curves for geometric modeling. *IBM J. Res. Develop.*, 1987, **31**(3), 296–313.
21. Sabin, M., The use of piecewise forms for the numerical description of shape. PhD Thesis, Hungarian Academy of Sciences, 1976.
22. Shani, U. and Ballard, D., Spline as embedding for generalized cylinders. *Computer Vision, Graphics, and Image Processing*, 1984, **27,** 129–156.
23. Sharrock, T. J., Biarcs in three dimensions. *The Mathematics of Surfaces II*, ed. R. R. Martin. Clarendon Press, Oxford, 1987, pp. 395–411.
24. Shoemake, K., Animating rotation with quaternion curves. *Proceedings of SIG-GRAPH '85*, 1985, pp. 245–254.
25. Siltanen, P. and Woodward, C., Normal orientation methods for 3D offset curves, sweep surfaces, skinning. *EUROGRAPHICS '92*. Blackwell Publishers, 1992, pp. 449–457.
26. Su, B. Q. and Liu, D. Y., *Computational Geometry: Curve and Surface Modeling*. Academic Press, San Diego, 1989.
27. Wang, W., Results on conics and quadrics in computer aided geometric design. PhD Thesis, Department of Computing Science, University of Alberta, Canada, 1992.
28. Wang, W. and Joe, B., Classification and properties of space biarcs. *SPIE Conference Proceedings: Curves and Surfaces in Computer Vision and Graphics III*, Boston, Nov. 1992.
29. Wang, W. and Joe, B., On approximation degree of biarc interpolation. Submitted for publication.
30. van Wijk, J. J., Ray tracing objects defined by sweeping planar cubic splines. *ACM Transactions on Graphics*, 1984, **3**(3), 223–237.

*Wenping Wang is an assistant professor of computer science. He received a PhD in computer science from the University of Alberta, Canada, in 1992. His research interests include computer graphics, geometric modeling and computational geometry.*

*Barry Joe is an associate professor. He received a PhD in computer science from the University of Waterloo, Canada, in 1984. His research interests include 2D and 3D finite-element mesh generation, mathematical software, computational geometry, geometric modeling, and computer graphics.*